J. Condensed Matter Nucl. Sci. 13 (2014) 471–484

Research Article

Hydrogen Isotope Absorption and Heat Release Characteristics of a Ni-based Sample

H. Sakoh, Y. Miyoshi, A. Taniike, Y. Furuyama and A. Kitamura*, †

Graduate School of Maritime Sciences, Kobe University, Higashinada-ku, Kobe 6580022, Japan

A.Takahashi‡, R. Seto and Y. Fujita

Technova Inc., Chiyoda-ku, Tokyo 1000011, Japan

T. Murota and T. Tahara

Santoku Corp., Higashinada-ku, Kobe 6580013, Japan

Abstract

Recently, several researchers have claimed excess heat from Ni-based alloy nano-compound samples during gas-phase protium absorption. nickel is used instead of expensive Pd-based nano-compounds. We have performed hydrogen isotope absorption runs using the Cu–Ni–ZrO_2 and Ni–ZrO_2 nano-powders. We observed long-lasting temperature changes corresponding to astonishingly large output energy of several hundred eV/atom-Ni.
 ISSN 2227-3123

Keywords: Catalyst, Cu–Ni alloy nano-powder, Protium absorption

1. Introduction

Rossi and Focardi reported large heat generation on the order of kilowatts from a Ni-based alloy powder sample absorbing protium (H)–gas at elevated temperatures above 573 K [1]. Brian Ahern (private communication) infers that their sample would be a mixture of nickel and copper.

In contrast to these dramatic reports, our Ni–ZrO_2 samples did not show any appreciable absorption of hydrogen isotopes or heat release at room temperature [2,3]. Pd_1Ni_7 nano-particles dispersed in a ZrO_2 substrate, supplied by B. Ahern, showed a dramatic change in the amount of absorbed hydrogen to very large values [4–6] at room temperature.

*E-mail: kitamuraakira3@gmail.com
†Also at: Technova Inc., Chiyoda-ku, Tokyo 1000011, Japan.
‡Also at: Osaka University, Suita 5650871, Japan.

 ISSN 2227-3123

Table 1. Characteristics of the NZ and CNZ samples.

	CNZ			NZ	
	Cu	Ni	Zr	Ni	Zr
Specific surface area (m^2/g)	25.3			20.6	
Composition (%)	7.9	36.0	56.1	35.8	64.2
Average grain size (nm)	6.8	24.5	–	23.2	–

This result gives a strong indication that significant improvement of absorption characteristics would be expected by adding a small amount of foreign atoms to the Ni–Zr sample.

In the present work, we used compounds of Ni–Zr mixed oxide (NZ) and Cu–Ni–Zr mixed oxide (CNZ) nano-powders fabricated by Santoku Corporation as samples for hydrogen isotope absorption experiments.

2. Experimental Apparatus and Procedure

The physical properties of the NZ and CNZ samples are shown in Table 1. Figure 1 shows a schematic of one part of the twin system. We have used a twin absorption system consisting of two equivalent chambers for hydrogen isotope gas absorption/adsorption experiments. The nickel samples are put in the reaction chambers, which are evacuated through filters to eliminate particles of sizes greater than about 5 μm. They are baked, to outgas them. The outer chambers are evacuated in order to thermally insulate the inner chamber during hydrogen isotope absorption/adsorption. Sheath heaters with resistance of 37.9 and 53.8 Ω are wound around the reaction chambers in the A_1 and A_2 systems, respectively. These are used to bake the sample before the run, and to heat it during runs at elevated temperatures.

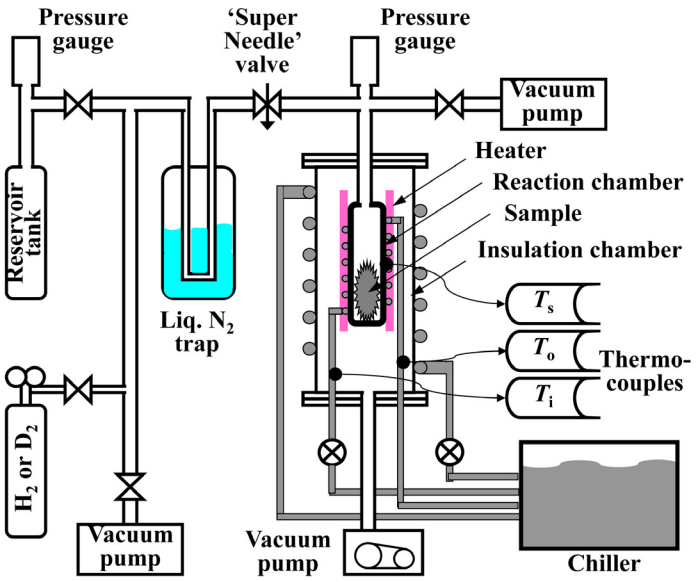

Figure 1. Functional view of the system $A_1 \cdot A_2$. Water cooling of the reaction chamber with a flow rate of 6 ml/min was done only in the #1 run at room temperature. The cooling water pipe was empty in the #5 runs at elevated temperatures.

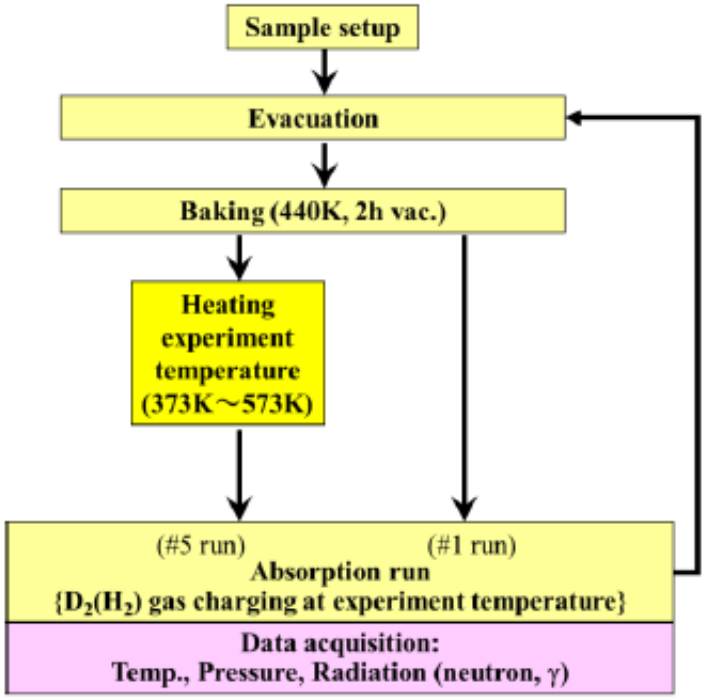

Figure 2. Flow-chart of the experimental procedure.

Alumel-chromel thermo-couples are used to measure temperatures. To reduce the influence of environmental temperature changes as small as possible, only the outer vacuum vessel was cooled with water at constant temperature

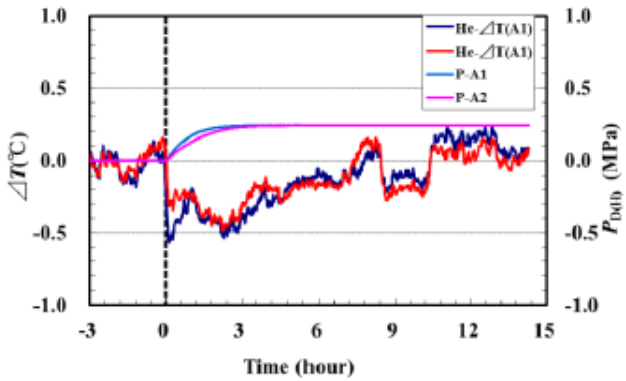

Figure 3. Variation of temperature and pressure in the blank runs with ^{4}He gas, at an input power of 70 W by the heater.

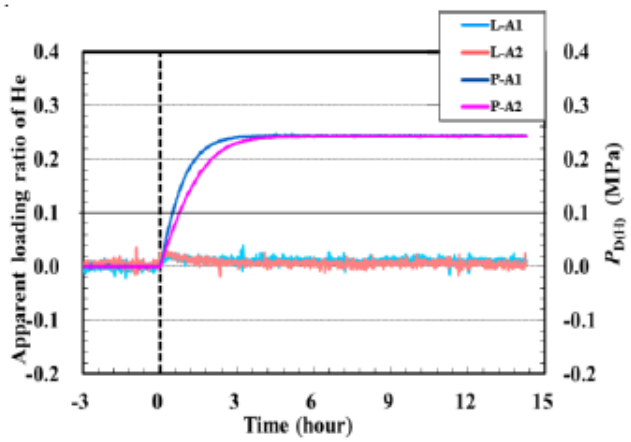

Figure 4. Pressure and apparent loading ratio in the blank run with ^{4}He gas at an input power of 70 W from the heater.

(regulated within 0.1°C variation), and the experimental room was air-conditioned to keep temperature change within 0.1°C variation.

Figure 2 shows the experimental procedure. The reservoir tank is filled with D_2 (H_2) gas at a pressure of 0.3 MPa, typically, before an absorption run starts. The reaction chamber and the outer chamber are evacuated, and the coolant water is run. The reaction chamber is then heated to a prescribed temperature. When the chambers attain the constant temperature, the D_2 (or H_2) gas is run with a flow rate adjusted and regulated with a "Super Needle" valve.

Blank runs for isothermal calorimetry were performed, with ohmic heating and ^{4}He gas charging instead of H(D)-gas. This data was used to correct the time-evolution data for the temperature and the pressure in the reaction chamber. Time variation of input power was recorded and used to correct the calorimetry. Any fluctuation of the temperature of

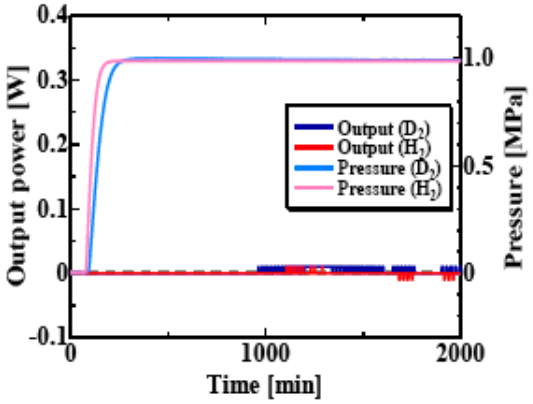

Figure 5. Results of D_2/H_2 absorption runs for Ni–Zr oxide compounds; the run numbers are D–NZ1#1 and H–NZ2#1.

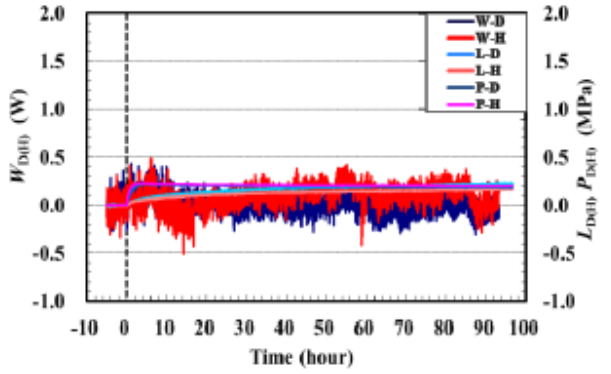

(**a**)

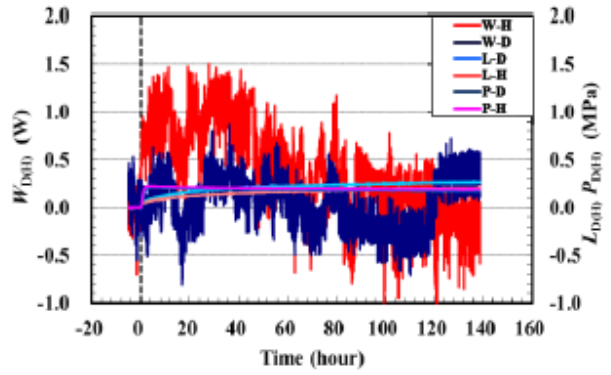

(**b**)

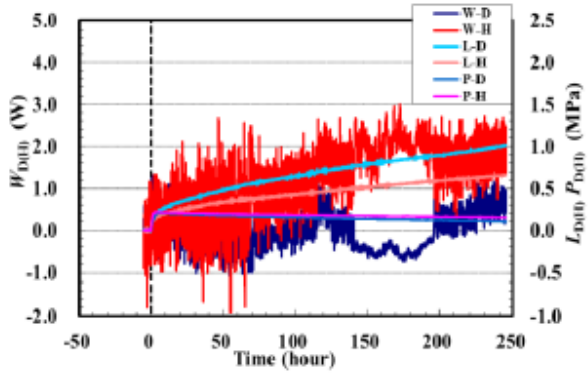

(**c**)

Figure 6. Variation of the thermal output power $W_{D(H)}(t)$, the pressure $P_{D(H)}(t)$ and the time-dependent loading ratio $L_{D(H)}(t)$ in the runs (a) H(D)–NZ3(4)#5_473 K, (b) H(D)–NZ3(4)#5_523 K and (c) H(D)–NZ3(4)_573 K.

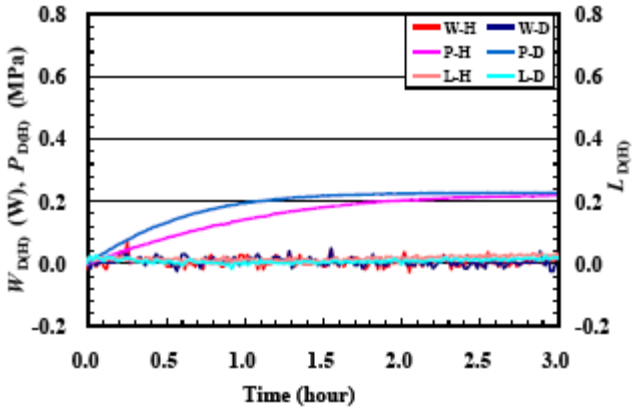

Figure 7. Evolution of the thermal power $W_{D(H)}$, pressure $P_{D(H)}$ in the reaction chamber after introduction of D_2 (or H_2) gas and the time-dependent loading ratio $L_{D(H)}$ in runs D–CNZ1#1 and H–CNZ2#1.

the reaction chamber not coincident with an intentional change in the heater input power is regarded as a maximum error, and was evaluated to be ±0.5 W at 573 K. An example of such fluctuations is seen in Fig. 3.

The instantaneous amount of absorbed hydrogen atoms in each reaction chamber can be calculated by measuring the pressures of both the reaction chamber and the reservoir tank. Since the gas is supplied through the valves and pipes at room temperature, there is an apparent emission (or negative loading) of the gas from somewhere in the reaction chamber due to expansion by heating. The apparent helium loading ratio, which should be negligible, is minimized by suitably approximating the temperature distribution in the "reaction chamber" consisting of the bottle itself and the pipes downstream of the Super Needle.

An example of the apparent loading ratio $L_{D(H)}(t)$ in the blank run using ^{4}He at a heating power of 70 W is shown in Fig. 4. We use the marginal apparent loading ratio of helium to estimate the systematic error, to correct the loading ratios in the hydrogen absorption runs.

The temperature measurement is also affected by the introduction of cool gas. Therefore, blank runs in which ^{4}He gas was introduced into the reaction chamber under the same experimental conditions as in the cases of the hydrogen runs were necessary. Figure 3 is an example of a blank run using ^{4}He operated at 70 W. The fall of temperature, with the difference in the heat capacity of ^{4}He (20.8 J/mol K) and $D(H)_2$ (28.8 J/mol K) taken into account, is used for correction in the data processing to obtain the thermal output power $W_{D(H)}(t)$.

The relation between the evolving thermal power and the temperature was obtained beforehand. The temperature of the reaction chamber was measured for the heater input powers of 0, 15, 27, 43.5, 70, and 105 W. The results are shown in Table 2. Linear interpolation using the derivatives, $\Delta T/\Delta W$ values, is applied for an arbitrary value of the temperature other than the temperatures measured in the calibration. We estimated there is a ±0.2 W systematic error in the calorimetry.

There is a delay in the response of the temperature. The transition curve is well approximated by a two-component exponential function with a time constant of 16 min and 45 min, each corresponding to thermal energy losses due to radiation and conduction.

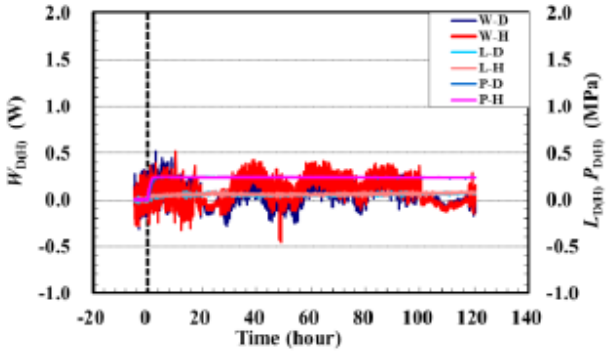

(**a**)

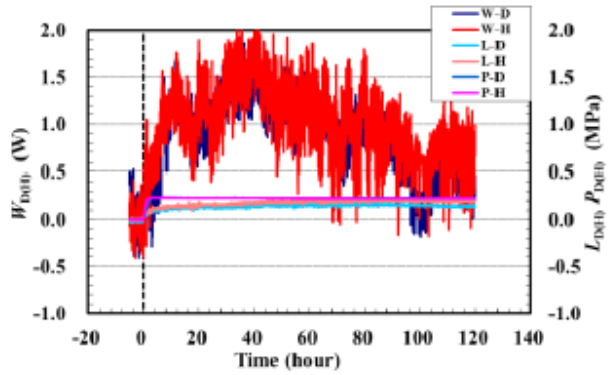

(**b**)

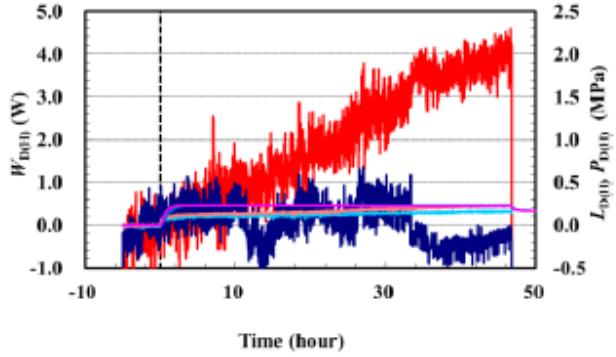

(**c**)

Figure 8. Variation of the thermal output power $W_{D(H)}(t)$, the pressure $P_{D(H)}(t)$ and the time-dependent loading ratio $L_{D(H)}(t)$ in the runs (a) H(D)-CNZ3(4)#5_473 K, (b) H(D)-CNZ3(4)#5_523 K, and (c) H(D)-CNZ3(4)#5_573 K_2.

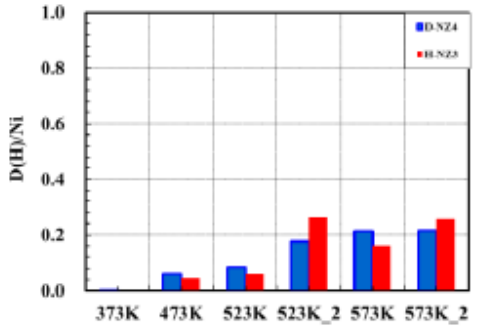

(a)

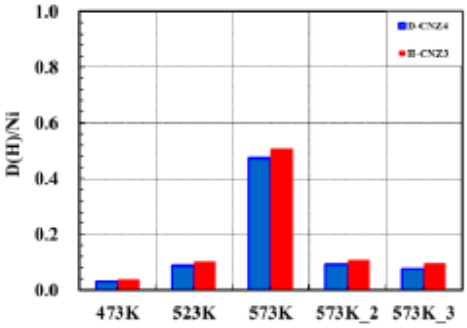

(b)

Figure 9. H(D)/Pd data for the t-phase of sample H(D)–NZ, upper figure (a) and H(D)– CNZ, lower figure (b).

3. Experimental Results

Figure 5 shows typical variation of the heat output, $W_D(t)$ and $W_H(t)$, pressure in the reaction chamber, $P_D(t)$ and $P_H(t)$, in the hydrogen isotope absorption run at 293 K for as-received samples, D-NZ1 and H-NZ2, respectively. We observed negligible absorption of hydrogen isotopes accompanied by exothermic temperature change, confirming that nickel does not absorb hydrogen at room temperature [7].

Activation of the H(D)-gas absorption reaction is expected at higher temperatures. Therefore, the experiments were

Table 2. Relation between the temperature of the reaction chamber and the heater input power for each subsystem, A_1 and A_2. The differential value $\Delta T/\Delta W$ is the slope of the line connecting the neighboring points.

Input power (W)	T (K)		$\Delta T/\Delta W$ (K/W)	
	A_1	A_2	A_1	A_2
0	294.2	294.2	–	–
15	393.3	388.2	6.61	6.27
27	435.9	429.3.	3.55	3.43
43.5	480.7	472.1	2.72	2.59
70	524.5	523.2	1.65	1.93
105	564.4	565.5	0.99	0.99

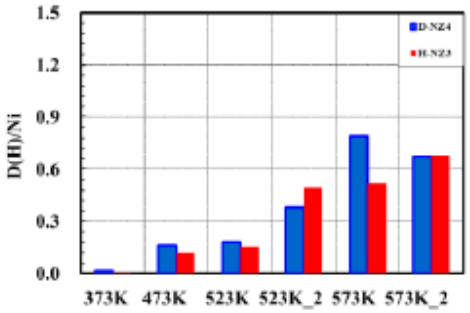

(**a**)

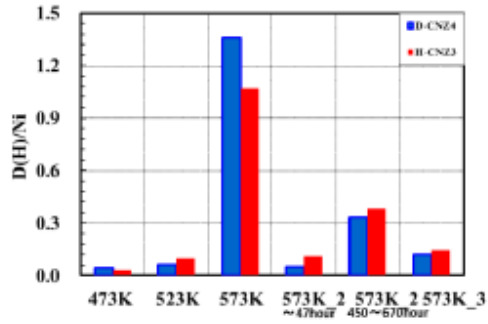

(**b**)

Figure 10. H(D)/Pd data for the s-phase of sample H(D)–NZ, upper figure (a) and H(D)– CNZ, lower figure (b).

also conducted at elevated temperatures up to 573 K with use of the heater input power of up to 105 W. Figures 6(a)–(c) show typical variation of the heat output, $W_{\mathrm{D}}(t)$ and $W_{\mathrm{H}}(t)$, pressure in the reaction chamber, $P_D(t)$ and $P_{\mathrm{H}}(t)$, and the loading ratio, $L_{\mathrm{D}}(t)$ and $L_{\mathrm{H}}(t)$, in the hydrogen isotope absorption runs, H(D)–NZ1(2)#5_373 K through H(D)–NZ1(2)_573 K, respectively.

At 473 K, we did not observe an appreciable exothermic reaction. In the protium absorption run at 534 K an exothermic reaction with the maximum output power exceeding 1.0 W was registered. Although it is only a small change compared with the input heater power of 70 W, it continued for about 40 h.

In the protium run at 573 K, the power increased gradually to reach about 2 W, and the exothermic reaction continued for 250 h. However, the sample absorbed/adsorbed deuterium with much less output power, sometimes even endothermically. The loading ratio was larger than in any other run. The D/Ni ratio reached 1.0.

We cannot distinguish absorption from adsorption with our present configuration. We admit that the "absorption" could include protium moving not only into interstitial sites but also into vacancies and vacancies clusters. However, it is hardly imagined that the sample has vacancies to accommodate hydrogen atoms as much as more than 10% of the host lattice atoms. It is natural therefore that the most hydrogen atoms are absorbed into the interstitial sites or adsorbed on the surfaces. In the following we mean "absorption and/or adsorption" by "absorption".

The exothermic reaction was more prominent in the protium runs than in the deuterium runs in almost all cases including the helium blank runs.

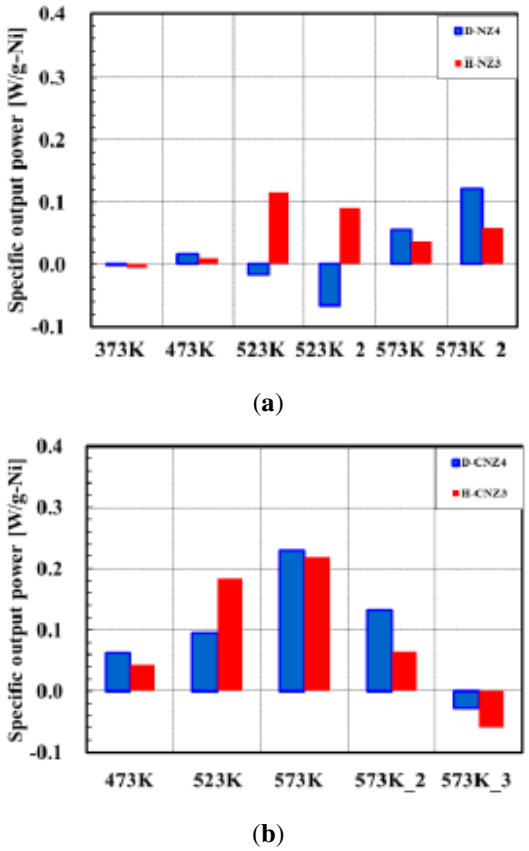

Figure 11. Specific output power data for the t-phase of sample H(D)–NZ, upper figure (a) and H(D)–CNZ, lower figure (b).

However, the system appears to lose long-term stability at temperatures higher than 500 K. The above temperature change regarded as the exothermic reaction is rather small, at most only about 2% of the input power. We are not very confident that it indicates a real exothermic reaction.

Next, the hydrogen absorption characteristics of the CNZ sample is described. Figure 6 shows the temporal behavior of the absorption parameters in the room temperature runs, D–CNZ1#1 and H–CNZ2#1. We have not observed absorption of hydrogen nor exothermic temperature change similarly to the NZ sample. We stopped the runs before we were able to collect much data, because we wanted to finish a certain number of experimental runs on a tight schedule.

After the #1 run, we performed hydrogen isotope absorption runs under conditions similar to the NZ sample. Figures 7(a)–(c) show the absorption parameters in the runs, H(D)–CNZ3(4)#5_473 K through H(D)–CNZ3(4)_573 K. At 473 K, we did not observe an exothermic reaction like the one we saw with the NZ sample. At 523 K the exothermic reaction appeared both in the protium and deuterium runs and continued for more than 100 hours. The power increased gradually to reach about 2 W.

At 573 K the sample absorbed gas-phase protium, and produced output power of 4.0 W maximum. This is twice as large as that of the NZ sample at the same temperature. Granted, it is only a small amount of power compared with

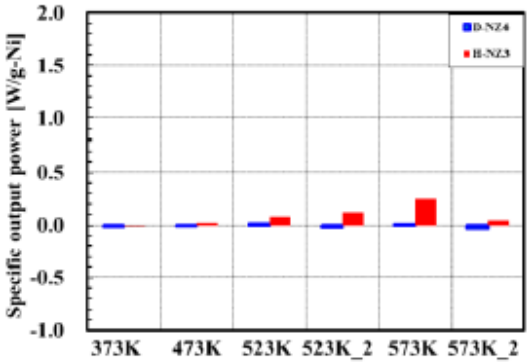

(**a**)

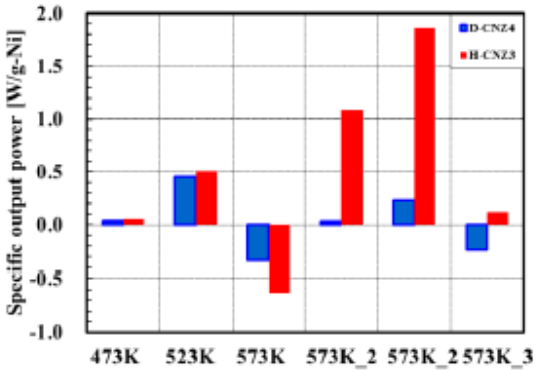

(**b**)

Figure 12. Specific output power data for the s-phase of sample H(D)–NZ, upper figure (a) and H(D)–CNZ, lower figure (b).

the input heater power. Note that the NZ sample had 5.41 g of net Ni, while the CNZ sample had 2 g of net Ni.

In evaluating the time-integrated output energy, we take notice of the fact that the CNZ-sample runs have an initial phase in which appreciable absorption takes place. We call this the t-phase, and distinguish between it and the rest of the run which has almost constant pressure. We call the latter the s-phase. The specific output energy $E_{\mathrm{D(H)}}$ (eV/atom-Ni) is evaluated by integrating the specific output power $W_{\mathrm{D(H)}}$ (W/g-Ni) until the time when the power becomes either almost zero or some constant value.

Figures 9, 11 and 13 are the histograms showing the loading ratio H(D)/Pd, the mean specific output power $W_{\mathrm{D(H)}}$, and the specific output energy $E_{\mathrm{D(H)}}$ in the t-phase of the four runs operated at temperatures 373–573 K. Figures 10, 12 and 14 are those in the s-phase of these runs. In Fig. 14 for $E_{\mathrm{D(H)}}$, the integration times are shown in parentheses in the line below the x-axis.

The loading ratio for the sample CNZ is almost the same as that for the NZ sample both in the t-phase and the s-phase. On the other hand, the mean specific output power and the specific output energy for the CNZ sample are larger than those for the NZ sample operated at temperatures higher than 500 K. Especially, the specific output energy E_H reached about 800 eV/atom-Ni for the CNZ sample at 573 K, which is too high to be explained by any known

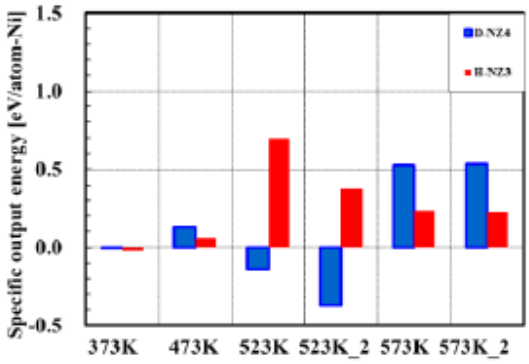

(**a**)

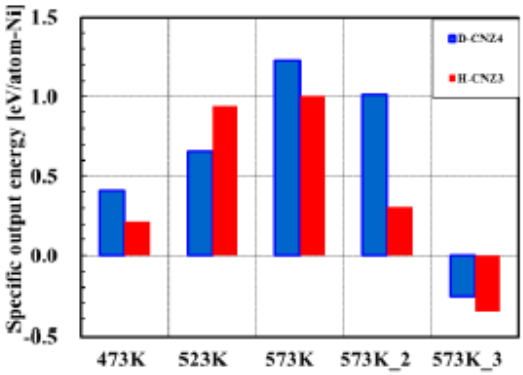

(**b**)

Figure 13. Specific output energy data for the t-phase of sample H(D)–NZ, upper figure (a) and H(D)–CNZ, lower figure (b).

chemical processes. The reason is as follows. All chemical processes including oxidation and de-oxidation proceed by exchanging outer electrons having binding energies at most 10 eV.

Therefore, we hardly suppose any atomic/molecular reaction energy greater than 10 eV/atom-H or 10 eV/atom-Ni. We admit that the oxygen pick-up reactions could be included. However, the reaction energies are lower than 1 eV or even negative; $NiO + H_2 \rightarrow Ni + H_2O + 0.7$ eV, $ZrO_2 + 2H_2 \rightarrow Zr + 2H_2O - 6.4$ eV.

Based on our results, we conclude that the copper atoms act as catalysts to produce the heat release under hydrogen isotope absorption/adsorption, presumably by substantially deepening the potential for interstitial hydrogen atoms inside nano-particles and/or surface atomic hydrogen. How the deeper potential relates to the nuclear reaction is the core question. We do not have the answer at the moment. A possible answer might be the Takahashi model [8].

In view of the large fluctuations of the observed temperatures, cautious reexamination of the absorption runs with a larger amount of the nickel sample material is necessary to confirm what appears to be continued, extraordinary large heat evolution.

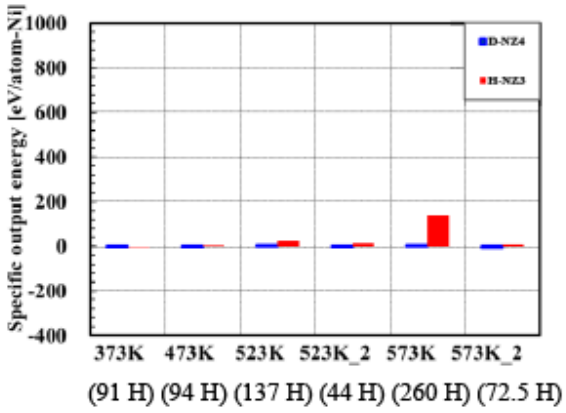

(**a**)

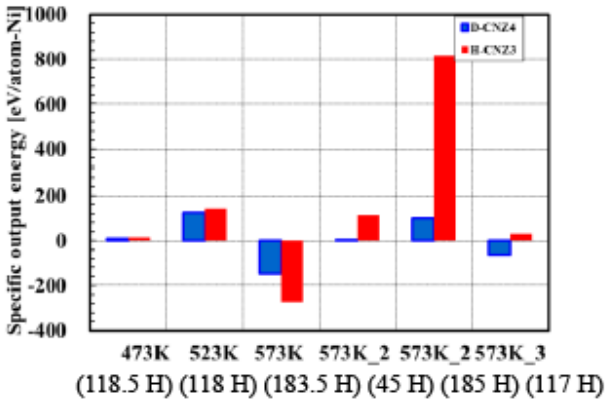

(**b**)

Figure 14. Specific output energy data for the s-phase of sample H(D)–NZ, upper figure (a) and H(D)–CNZ, lower figure (b). The duration (integration time) of each run is designated below the temperature of the run in parenthesis.

4. Conclusion

The results of the present work are summarized as follows:

(1) Both NZ and CNZ samples showed apparent heat release at temperatures higher than 500 K.
(2) Absorption of protium is more effective than deuterium absorption at producing a heat release.
(3) The loading ratio for the NZ sample was almost the same as that for the CNZ sample, while for the heat release the CNZ sample was ten times more effective than the NZ sample. We infer that the copper atoms act as a catalyst for hydrogen absorption of the nickel nano-particles to deepen the potential well for the adsorption/absorption.

(4) As the sample temperature was raised, the heat release and the loading ratio became larger. It may be possible that the sample will show an even larger heat release and a larger loading ratio at temperatures above 573 K.

References

[1] For example, http://en.wikipedia.org/wiki/Energy_Catalyzer.
[2] Y. Sasaki, Y. Miyoshi, A. Taniike, A. Kitamura, A. Takahashi, R. Seto and Y. Fujita; *Proc. JCF10,* 2010, pp. 14–19.
[3] A. Kitamura, Y. Miyoshi, A. Taniike, A. Takahashi, R. Seto and Y. Fujita, *J. Condensed Matter Nucl. Sci.* 4 (2011) 56–68.
[4] B. Ahern, private communication.
[5] H. Sakoh, Y. Miyoshi, A. Taniike, A. Kitamura, A. Takahashi, R. Seto and Y. Fujita, *Proc. JCF11*, 2011, pp. 16–22.
[6] Y. Miyoshi, H. Sakoh, A. Taniike, A. Kitamura, A. Takahashi, R. Seto and Y. Fujita, *Int. Conf. on Condensed Matter Nuclear Science, ICCF16*, Chennai, 2011, paper MT-02.
[7] Y. Fukai, K. Tanaka and H. Uchida, Hydrogen and Metals (Uchida Rokakuho, Tokyo, 1998) (in Japanese).
[8] A. Takahashi, *J. Condensed Matter Nucl. Sci.* **9** (2012) 108.